Efficient removal of uranium, cadmium and mercury from aqueous solutions using grafted hydrazide-micro-magnetite chitosan derivative

Mohammed Hamza, Yuezhou Wei, Asmaa Benettayeb, Xinpeng Wang, Eric Guibal

Efficient removal of uranium, cadmium and mercury from aqueous solutions using grafted hydrazide-micro-magnetite chitosan derivative

Mohammed F. Hamza[1,2,3], Yuezhou Wei[1,4,*], Asmaa Benettayeb[5], Xinpeng Wang[1], and Eric Guibal[2,*]

[1] *Guangxi Key Laboratory of Processing for Non-Ferrous Metals and Featured Materials, School of Resources, Environment and Materials, Guangxi University, 100 Daxue Road, Nanning 530004, Guangxi, People's Republic of China*

[2] *C2MA, IMT – Mines Ales, Univ. Montpellier, 6 avenue de Clavières, 30319 Alès Cedex, France*

[3] *Nuclear Materials Authority, POB 530, El-Maadi, Cairo, Egypt*

[4] *Shanghai Jiao Tong University, Dongchuan Rd. 800, Shanghai, People's Republic of China*

[5] *Laboratoire de Génie Chimique et de Catalyse Hétérogène, Université de Science et de la Technologie – Mohamed Boudiaf, Oran, Algeria*

ABSTRACT

Magnetic chitosan microparticles are functionalized by grafting a new hydra-zide derivative to produce HAHZ-MG-CH, which is applied to the sorption of metal cations. The functionalization (appearance of new groups) and synthesis mechanisms are confirmed using elemental analyses, FTIR and XPS spectrom-etry, TGA and EDX analysis, SEM observation and titration. HAHZ-MG-CH bears high nitrogen content ($\approx$ 10.9 mmol N g^{-1}). Maximum sorption capaci-ties at pH 5 reach up to 1.55 mmol U g^{-1}, 1.82 mmol Hg g^{-1} and 2.67 mmol Cd g^{-1}. Sorption isotherms are preferentially fitted by the Langmuir model. In acidic solutions, the sorbent has a marked preference for Hg(II) over U(VI) and Cd(II), while at mild pH uranyl species are preferentially bound. The sorbent has a lower affinity for Cd(II) in multicomponent solutions. Sorption occurs within 60 min of contact. The pseudo-first-order rate equation fits well kinetic profiles. HCl solutions (0.5 M) successfully desorb all the metal ions (yield exceeds 97% at the first cycle). The sorbent can be recycled for 5 cycles of sorption and desorption: the loss in efficiencies does not exceed 8%. The sorbent removes Hg(II), Cd(II) and Pb(II) from local contaminated groundwater at levels compatible with irrigation and livestock uses but not enough to reach the levels for drinking water regulations.

Address correspondence to E-mail: yzwei@gxu.edu.cn; eric.guibal@mines-ales.fr

Introduction

The removal of metal ions from wastewater and from industrial effluents is a critical topic of research in link with two growing demands from the community and from governmental and international institutions [1]. Indeed, the discharge of heavy metals may cause serious health threats and damages to the biotope. On the other hand, the increasing demand for valuable metals make necessary recycling as much as possible spent metal resources (recovery from spent materials, valorization of sub-products). Environmental regulation and recycling policies are then important catalysts for the development of new processes for metal recovery.

Many processes were developed for metal removal including precipitation [2], solvent extraction [3], electrolytic techniques [4] and membrane technologies [5]. However, they frequently face technical or economical limitations for the treatment of low-concentration effluents containing a large variety of metal ions. There is still a need for developing alternate processes, and sorption is an expanding research area for developing new materials addressed to the recovery of heavy metals from dilute solutions. Hence, ion-exchange and chelating resins have received a great attention in the last decades [6–11]. Chemically modified minerals were also efficiently designed for metal sorption [12]. New materials have been recently developed for increasing sorption capacities or improving uptake kinetics such as polymer brushes [11, 13] or metal organic frameworks (MOFs) [14]. Functionalized activated carbons and multi-walled carbon nanotubes have also retained attention for the last decades [15, 16]. Biosorbents were deeply investigated to substitute synthetic resins with renewable resources [17–25]. The binding mechanisms are based on the reactivity of the same functional groups as those found on resins: chelation and ion-exchange mechanisms occur on naturally present reactive groups or on grafted moieties. Chitosan (obtained by partial deacetylation of chitin, one of the most abundant polysaccharide) has received a great attention because of its hydrophilic nature and the presence of amine functions [26]: metal cations can be bound by chelation on lone electron pair of nitrogen in near-neutral solutions, while metal anions can be sorbed onto protonated amine groups in acidic solutions [27–29]. Metal transfer is controlled by the resistance to intraparticle diffusion because the polymer is poorly porous; this makes necessary modifying its structure by manufacturing hydrogels with expanded structure [30, 31]. An alternate solution for improving mass transfer consists of depositing thin layers of biopolymer at the surface of inactive supports [32–34]. The synthesis of composite magnetic/chitosan supports of micron- or nanometer size is an attractive alternative abundantly documented for preparing highly efficient and fast sorbents [35–38]. The coating of chitosan on magnetite particles may be a solution; however, the one-pot co-precipitation of chitosan with magnetite seems to be more appropriate for managing this kind of small-size objects. This is the solution preferred in this work. Another interest of chitosan is its readily chemical modification due to the reactivity of hydroxyl and amine groups [39–41]. The chemical modification of magnetic chitosan microparticles by grafting new functional groups allows combining fast sorption processes with high reactivity and/or selectivity [42, 43]. A new kind of hydrazide derivative of chitosan (supported on magnetic nanoparticles) has been designed in this work and tested for the sorption of heavy metals (including U(VI), Cd(II) and Hg(II)). These metals were selected because of their different speciation behavior (in terms of formation of polynuclear species for U(VI), formation of chloro-anionic species for Hg(II) and free species for Cd(II)). The study extensively characterizes the structure and chemical properties of the material before evaluating the sorption properties considering the effect of pH, the uptake kinetics and the sorption isotherms. Metal desorption and sorbent recycling are investigated before studying selectivity issues and testing the decontamination of a groundwater sample containing heavy metals.

Materials and methods

Materials

Chloride salts of cadmium and mercury (i.e., $CdCl_2$ and $HgCl_2$, Sigma-Aldrich, Taufkirchen, Germany) were used for preparing heavy metal stock solutions (1 g metal L^{-1}) by dissolving in Milli-Q water. SPEX Europe (Stanmore, UK) supplied the standard solution of depleted uranium (10 g U L^{-1}, SPEX CertiPrep, nitric acid solution). Metal ion solutions were

prepared by dilution of stock solutions in Milli-Q water prior to use (with appropriate pH control). The speciation of the metals may be influenced by the salt used and the acid and base used for pH control. The speciation diagrams plotted in the Additional Material Section (AMS) take into account the specific experimental conditions used for the study of pH effect. The limit pH values for precipitation have been considered (taking into account the salt used) and analyzed through speciation calculation to be sure that precipitation phenomena did not occur under selected experimental conditions.

Chitosan (deacetylation degree: 90.5%, commercial information), ethyl bromoacetate and acetone were supplied by Sigma-Aldrich (Taufkirchen, Germany) and used as received. Hydrazine hydrate, absolute ethanol and epichlorohydrin were obtained from Fluka AG (Switzerland). Other reagents were supplied by Prolabo (VWR, France).

Synthesis of sorbent

The synthesis procedure of hydrazinyl derivative was inspired by previous work on functionalization of magnetic chitosan microparticles [44]. The synthesis consists of five steps: (1) synthesis of magnetite/chitosan particles (MG-CH), (2) activation of the composite material through epichlorohydrin grafting (EPI-MG-CH), (3) grafting of nitrile functions (CN-MG-CH), (4) hydrazinyl amination (HA-MG-CH) and (5) hydrazide synthesis (HAHZ-MG-CH). The different steps of the synthesis are briefly reported in the Additional Material Section (Section I. AMS). The last step in the functionalization is described below. The procedure was modified for improving support functionalization; ester was substituted with ethyl bromoacetate for the grafting of hydrazinyl amine functions (Section II, see AMS) (compared with previous procedure [44]). Scheme 1 shows the proposed steps for the functionalization of the sorbent.

First, HA-MG-CH was reacted with a mixture of ethyl bromoacetate (14 g) and dry potassium carbonate (10 g) in 60 mL dry acetone. The mixture was maintained under agitation for 5 h at 65 ± 2 °C. After rinsing with acetone and Milli-Q water, the material (HACOEt-MG-CH) was freeze-dried. In a second step, the product was dropped into a mixture of 20 mL of absolute ethanol and 30 mL of hydrazine hydrate (60%, w/w). The reaction took place for 4 h, under reflux, to produce the hydrazide derivative HAHZ-MG-CH. The product was washed with ethanol and Milli-Q water before being freeze-dried.

It is noteworthy that at each step of the synthesis, the particles were magnetically separated before being transferred to the next functionalization step (from synthesis of magnetite chitosan particles to final functionalization).

Characterization of materials

FTIR spectrometry analysis was performed on KBr disk (finely ground dry sample pelletized in KBr, 1%, w/w) using a Shimadzu IRTracer-100 FTIR spectrometer (Tokyo, Japan). All the samples were dried at 60 °C before being analyzed. An element analyzer (2400 Series II CHNS/O elemental analyzer, Perkin-Elmer, Waltham, MA, USA) was used for the chemical analysis of the samples. The thermal decomposition of the materials (under N_2 atmosphere) was characterized on TG–DTA equipment (Netzsch STA 449 F3 Jupiter, NETZSCH-Gerätebau HGmbh, Selb, Germany). A scanning electron microscope (Phenom ProX SEM, Thermo Fisher Scientific, Eindhoven, Netherlands) was used for characterizing the morphology of the sorbent while the chemical composition was semiquantitatively analyzed by energy-dispersive X-ray analysis (integrated into the SEM system). A Tecnai G2 F30 S-TWIN/X-MAX 80 (Thermo Fisher Scientific, Hillsboro, OR, USA), working at a 300.0 kV accelerating voltage, was used for investigating the morphology and the size of nanoparticles. Dry samples were placed onto aluminum studs with carbon tape and sputter-coated with gold using an ion-sputtering instrument (SCB-12 Zhongke, China). Textural properties of samples (swept with N_2 gas for 4 h at 120 °C) were recorded on a Micromeritics TriStar II (Norcross, GA, USA) system at 77 K, using N_2 gas; data were treated using the BET equation (following BJH method). XPS spectra were obtained on an ESCALAB 250XI$^+$ instrument (Thermo Fischer Scientific, Inc., Waltham, MA, USA) that was calibrated using Ag $3d_{5/2}$ line (0.45 eV) and C 1s line (0.82 eV). The pH_{PZC} was obtained using the pH-drift method [45]: a fixed amount of sorbent (100 mg) was stirred for 48 h with 50 mL of 0.1 M NaCl solutions at different initial pH values (pH_0, in the range 1–14). The equilibrium pH was measured with a S220 Seven Compact pH/

Scheme 1 Synthesis of HAHZ-MG-CH.

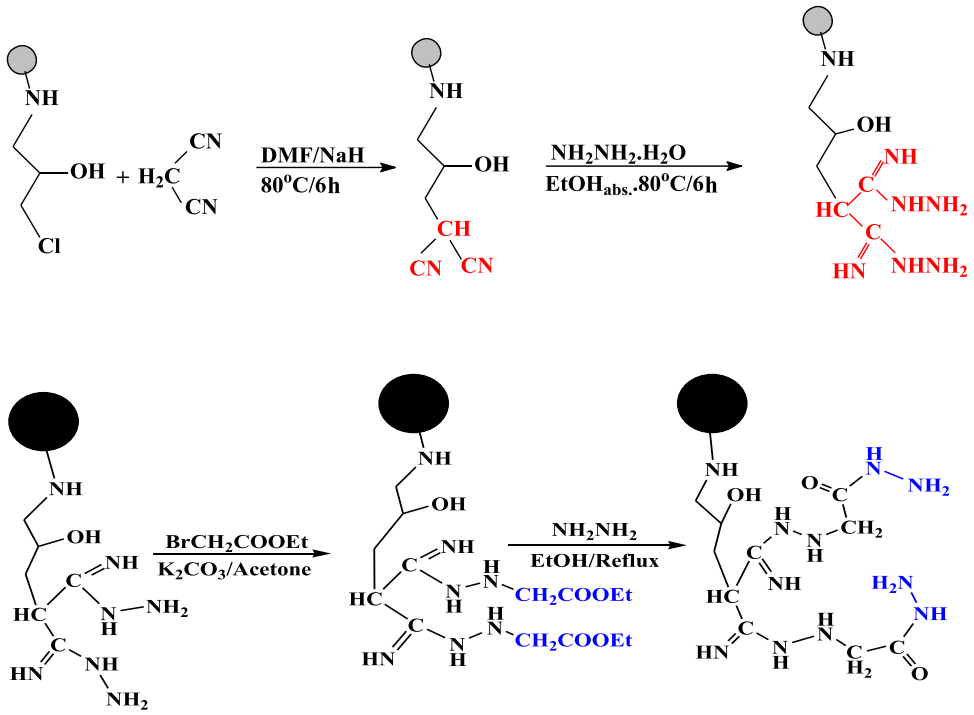

Ionometer. The pH_{PZC} corresponds to the value $pH_0 = pH_{eq}$.

Sorption tests

The specific experimental conditions are systematically reported in the caption of the figures and tables. The sorbent was mixed with a fixed volume of solution (V, L) containing a given concentration of metal ions (C_0, mg L^{-1} or mmol L^{-1}). The solid/liquid ratio selected for individual experiments was reported as sorbent dosage (SD); this is the amount of sorbent used per unit of volume (i.e., SD in mg or g of sorbent per L of solution). The pH was initially controlled with 0.1/1 M NaOH or HCl solutions for Cd(II) and Hg(II) solutions and with 0.1/1 M NaOH or HNO_3 solutions for U(VI); the pH was not adjusted during sorption, it was just monitored at the end of the experiment. For uptake kinetics, samples were regularly collected, filtrated on filter membrane (pore size membrane: 1.1 μm, or by magnetic separation) and the residual metal concentration was determined by inductively coupled plasma atomic emission spectrometer (ICP-AES JY Activa M, Horiba/Jobin-Yvon, Longjumeau, France). Sorption isotherms were obtained by contact of fixed amounts of sorbent (m, g) with given volumes (V, L; SD: 300 mg L^{-1}) of solutions of increasing initial metal concentration (C_0, mmol L^{-1}) at pH_0: 5.0, for 48 h. At equilibrium, the residual concentration (C_{eq}, mmol L^{-1}) was determined for calculating the sorption capacity (q_{eq}, mmol g^{-1}) by the mass balance equation: $q_{eq} = (C_0 - C_{eq}) \times V/m$. Section III (see AMS) shows the reproducibility tests: sorption performances are compared within the same sorbent stock and for two different stocks of sorbent.

Modeling of sorption isotherms and uptake kinetics

Uptake kinetics and sorption isotherms were modeled using conventional equations: the pseudo-first and the pseudo-second order rate equations [46], the resistance to intraparticle diffusion, (RIDE, the so-called Crank equation, [47]) and the Langmuir equation [48], respectively. The relevant equations are reported in Table AM1 (see AMS). The general shape of the sorption isotherms was characterized by a saturation plateau that allows rejecting the Freundlich model (power-like function [48, 49]). Parameters of the models were determined by non-linear regression analysis using Mathematica®.

Treatment of real metal-containing groundwater

The groundwater sample was collected in the Tora Hellwan area (Egypt), close to the Nile river (Figure AM1, see AMS). In the Ancient Egypt, this area was famous for the extraction of limestone and marbles; this is nowadays the most developed Egyptian site for cement production. This is a very contaminated area (both air and soil); this may explain unusually high levels of hazardous metals in local groundwater facilities. The study was focused on the removal of Hg(II), Cd(II), Pb(II) and Zn(II). Sorption tests were performed at four different initial pH0s: 2.0, 4.0, 6.2 and 7.0. The contact time was set at 1 h, and the sorbent dosage (SD) was 5 g L^{-1}. After filtration, the samples were analyzed and the residual concentration was used to calculate recovery efficiency. Residual concentrations were compared to maximum concentration levels acceptable for drinking water (MCL), feedstock and irrigation.

Note: The target metals selected in this study were chosen to illustrate the wide affinity of the sorbent for metals having different chemical profiles (especially in terms of speciation and affinity of functional groups). Mining effluents bearing uranium may contain cadmium but more rarely mercury. On the opposite hand, mercury and cadmium may coexist more frequently in industrial effluents. Therefore, the application process was tested on groundwater samples containing these two metals; application to uranium-bearing effluents will be part of a future work.

Results and discussion

Characterization of sorbents

Morphology—BET, SEM and TEM

The BET characterization of the sorbent showed a relatively low specific surface area: the SSA does not exceed 12 m^2 g^{-1}. This means that the material cannot be considered a highly porous material, despite the freeze-drying of the composite material that is expected to limit the irreversible collapse of the chitosan hydrogel structure (produced during the co-precipitation of the magnetite/chitosan composite). However, the precipitation of the biopolymer at the surface of magnetite micro/nanoparticles as a thin layer means that the resistance to intraparticle diffusion is not expected to strongly affect mass transfer properties (see below). TEM observations clearly show the presence of dense magnetite particles (Figure AM2, see AMS); their individual size roughly varies between 5 and 10 nm; although aggregates are formed as shown by SEM micrographs (Table AM2, see AMS): Particles are irregular in shape (ovoid shape with dimensions around 15 × 25 μm), with a rough surface.

Chemical composition—EDX and elemental analyses

Table AM3 (see AMS) shows the composition of the material (C, H and N contents) at the different steps of the synthesis of the sorbent. More specifically, the amount of N strongly increases from 1.3 mmol N g^{-1} on magnetic chitosan microparticles up to 10.86 mmol g^{-1} for HAHZ-MG-CH sorbent. Based on the expected synthesis pathway, the full substitution of amine groups would lead to a threefold increase in N content for CN-MG-CH, sevenfold increase for HA-MG-CH and 11-fold increase for HAHZ-MG-CH. These values are significantly different to those deduced from elemental analysis: the actual ratios are 3.77, 7.92 and 8.35, respectively. This means that the conversions from MG-CH to CN-MG-CH and HA-MG-CH are quantitative (and even in a slight excess), while the last step is much less efficient. The reaction at the last step may cause some degradation of amine groups bound on HA-MG-CH material, which, in turn, may affect the yield of conversion into HAHZ-MG-CH material. These ratios should thus be considered as purely indicative, but they show that the grafting of new reactive groups is highly efficient.

It is important to note that the loss on thermal degradation, at 660 °C, reaches up to 64.1%: magnetite represents about 36% of total weight. The semiquantitative analysis of the sorbent before and after metal ion was carried out using SEM–EDX facilities (Table AM4, see AMS). As expected, the main elements present on the support are: (a) Fe, representative of the magnetite core of the composite (close to 40%, w/w); (b) O, present in the polymer coating and magnetite representing about 30% (w/w), while (c) C and N elements represent the chitosan derivative deposited at the surface of magnetite microparticles. After sorption of uranyl ions, U signal

appears on EDX spectra (4.4%, w/w), in the case of Hg(II) and Cd(II) sorption, the binding of the heavy metal is also characterized by the appearance of substantial amounts of Cl, especially for Hg(II). Both mercury and cadmium were supplied as chloride salt; the presence of Cl is thus meaningful. However, it is important to observe that Hg(II) sorption is more efficient than Cd(II) binding (7% vs. 1%, w/w) and that Cl amount is also strongly increased in the case of mercury binding; this can be explained by the strong stability of chloro-mercuric complexes. The sorption of Hg(II) probably occurs through the binding of these chloro-complexes.

FTIR analysis

The analysis of the material at the different steps of the synthesis procedure allows identifying some specific and characteristics peaks assigned to functional groups or constituents of the composite material. The large band observed between 3500 and 3300 cm^{-1} (not shown) corresponds to the overlapping of –NH stretching vibrations (including primary, secondary groups) with –OH stretching vibration (including H-bonded groups); this band is weakly resolved and poorly exploitable for characterization of the materials. Figure AM3 (see AMS) shows selected wave number ranges on FTIR spectra for intermediary products and final sorbent. For example, the broad peak in the range 565–550 cm^{-1} (Fe–O stretching) is a clear identification of the magnetite core. The activation of the MG-CH material with epichlorohydrin can be confirmed by the shoulder at around 806 cm^{-1} (CH_2–Cl stretching) on EPI-MG-CH. The disappearance of this shoulder, during the grafting to form HA-MG-CH, confirms that the grafting operates on these functional groups. The nitrilation of EPI-MG-CH is also demonstrated by the appearance of the peak at 2360–2330 cm^{-1} (C≡N stretching) while after substitution of reactive groups the intensity of nitrile groups strongly decreases as a proof of effective grafting. The peak observed at around 1724 cm^{-1} on HACOOEt-MG-CH (associated to ethyl bromoacetate intermediary grafting) confirms the insertion of carbonyl groups (C=O stretching) of ester functions. The disappearance of this peak for HAHZ-MG-CH means that the substitution of hydrazide is highly efficient and effectively located on ethyl-carboxylate functions. The high density in amine groups (with different chemical environments) may also explain the large band and shifts for amine functions in the range 1650–1550 cm^{-1}. Table AM5 (see AMS) shows the shifts of the characteristic peaks, their assignments, and some relevant references. This summary confirms that the proposed mechanisms of synthesis (shown on Scheme 1) are consistent with FTIR analysis.

FTIR analysis can be also used for identifying the changes associated to metal binding (Figure AM4 and Table AM5, see AMS). The broad amine band (with maximum absorbance close to 1590 cm^{-1}) is shifted toward higher wave numbers for Cd(II)- and Hg(II)-loaded sorbents and to lower wavenumbers for U(VI)-loaded sorbent: Cd(II) and Hg(II) are following the same binding mechanism while U(VI) (uranyl species) may have a different mode of interaction with the sorbent. It is noteworthy that after metal desorption the spectrum of the sorbent was very close to the spectrum of the raw material: the sorbent globally remains stable after sorption/desorption operation.

XPS analysis

The material (HA-MG-CH) was analyzed by XPS before and after final functionalization (to form HAHZ-MG-CH) (Table AM6, see AMS) in order to follow the chemical changes and confirm the reaction pathway, but also before and after Cd(II) and Hg(II) sorption (Table AM7, see AMS). The signals of the main peaks are deconvoluted in order to identify the different functional groups but also their shifts during metal sorption: Table AM8 (see AMS) summarizes the main changes.

The analysis of C 1s signal allows identifying 4 peaks for HA-MG-CH, with binding energies, BEs: 284.04 eV, 285.67 eV, 287.46 eV and 287.9 eV, which correspond to (C–C, C–H), (C–NH, C–NH_2), (C(–O, =N), C–O–C), and O–C–O functional groups, respectively [50, 51]. The final functionalization of the material leads to limited shifts to 284.18 eV, 285.2 eV, 286.21 eV and 286.95 eV, respectively, but also to the appearance of a new peak assigned to amide group (O=C–NH) [52] at 287.86 eV. This is consistent with ethyl bromoacetate grafting and further hydrazide formation (also observed on its “cousin” derivative [44]). After metal sorption, the peak corresponding to carbonyl group of amide disappears. A tentative explanation can be proposed associated to the

tautomerization of carbonyl with amine group (Section IV, see AMS). Metal sorption involves electron sharing with carbonyl (and/or –OH) groups and amine groups; as a consequence the peaks referred to (C–C, C–H), (C–NH or C–NH_2), (C(–O, =N), C–O–C) and (O–C–O) are identified after Cd(II) binding at 283.95 eV, 285.43 eV, 285.87 eV and 287.67 eV, respectively. They are observed at 283.94 eV, 284.62 eV, 285.88 eV and 286.98 eV, respectively, after Hg(II) binding.

Three peaks are identified on N 1s spectrum of HA-MG-CH at 397.7 eV, 399.3 eV, and 400.0 eV, assigned to (NH-NH_2 or =NH), (C–N or NH_2) and (NH_3^+), respectively. After functionalization, the peaks are identified at 397.7 eV, 398.6 eV and 400.1 eV: the most significant change is observed on the band assigned to (C–N or NH_2), in addition to the appearance of a new peak at 401.73 eV, which is attributed to N in amide environment [35, 53, 54]. After metal binding the amide band disappears, in agreement with the tautomerization effect and the appearance of new N-metal bound peaks at 404.74 eV for Cd(II) and 400.36 eV for Hg(II). The peaks for (NH–NH_2 or =NH), (C–N or NH_2) and (NH_3^+) groups are reported at 398.18 eV, 398.72 eV and 399.85 eV in the case of Cd(II) binding and at 397.88 eV, 398.25 eV and 399.37 eV for Hg(II) binding. The coordination of metal ions with nitrogen may explain these shifts [55, 56].

The O 1s spectra of the materials show two families of peaks:

(a) the Fe–O groups associated to iron oxides (Fe_3O_4, as a mixture of Fe_2O_3 and FeO), whose BEs (deconvoluted in two peaks at 530 eV and 529 eV) are poorly affected by chemical modification and by metal sorption, and
(b) the C–O and or OH groups with a band observed at 532.7 eV (shifted toward 532.13 eV after chemical modification) [50].

With metal sorption, the carbonyl peak of amide group [57] disappears due to tautomerization effect and metal interaction; the bands relative to C–O and OH group are, respectively, shifted to 532.27 eV and 528.87 eV after Hg(II) sorption and to 532.13 eV, 529.2 eV after Cd(II) sorption. A new peak is observed at 532.32 eV (or at 532.2 eV) after Cd(II) binding (or Hg(II) binding); it is assigned to the direct interaction of the metal ion with O-ligand. This means that O-donor reactive groups are also involved in metal sorption [58, 59], in addition to N-based binding sites.

Consistently with previous observation on other magnetic supports also prepared by the Massart method [35], the XPS analysis of Fe 2p band confirms the coexistence of several oxidation states associated to Fe_3O_4 (Fe_2O_3 and FeO) [60]. Being part of the core of the material without limited interactions with the polymer and metal ions, the BEs of the typical bands Fe 2p remain almost unchanged. The magnetization saturation of the sorbent was not determined; however, the FTIR and XPS analyses allow identifying the presence of magnetite, which was also identified as dense nanoparticles in the core of sorbent particles by TEM.

The sorption of Cd(II) on the sorbent is confirmed by the appearance of Cd $3d_{3/2}$ and Cd $3d_{5/2}$ peaks, at 411.33 eV and 404.72 eV, respectively [58]. After Hg(II) sorption, two new peaks are also observed at 100.15 eV, and 104.47 eV, corresponding to Hg $4f_{7/2}$ and Hg $4f_{5/2}$, respectively. Identical peaks were identified in the case of Hg(II) binding (under the form of $HgCl_2$) [59]. Section IV (see AMS) shows tentative mechanisms of interaction between metal ions and functional groups.

TGA analysis

Three steps characterize the thermal degradation of the sorbent (Table AM9, see AMS) [36, 61]:

(a) from 19.12 to 191.17 °C, the mass loss reaches 9.84%; this corresponds to the elimination of adsorbed water.
(b) From 191.17 to 581.36 °C, the sorbent loses 31.98% of its weight (total cumulated mass loss reaches 41.82%); this is assigned to the dehydration of the saccharide ring and the degradation of the chitosan backbone. The degradation of the other organic moieties grafted on chitosan backbone may also occur in this range. However, it was not possible separating on TGA and derived curves the respective contributions of the thermal degradation of the different organic constituents. Madrid et al. [62] reported that the presence of amine functions slowed down the degradation of water hyacinth fibers; this was explained by the effect of radical scavenger of amine groups.

(c) From 581.36 to 801.79 °C, the mass loss is close to 22.99% (total cumulated mass loss up to 64.81%, consistently with the mass loss observed on sorbent burning at 660 °C; i.e., 64.1%). This phase is attributed to the degradation of the organic skeleton (including the char), and the phase change of magnetite to a lesser extent.

pH_{PZC}

The pH-drift method shows that the pH_{PZC} is close to 5.61 (Figure AM5, see AMS). This is important for predicting the protonation of reactive functional groups. At pH below 5.61, the amine groups hold on the sorbent are protonated; this induces a repulsion effect for the binding of metal cations. While the pH increases, the protonation progressively decreases the repulsion effect diminishes. This contributes to enhancing the sorption of metal cations. On the other hand, depending on the composition of the solution and the speciation of metal ions, the formation of anionic metal complexes may facilitate their sorption in acidic solutions. This value of pH_{PZC} is much lower that the value obtained with another hydrazinyl amine derivative of magnetic chitosan (i.e., pH_{PZC}: 7.87) [35]. This is probably due to the higher density of amine functions.

Sorption properties

pH effect

Figure 1 compares the effect of pH on U(VI), Hg(II) and Cd(II) sorption capacities using HAHZ-MG-CH sorbent. As expected, increasing the pH improves the sorption efficiency: the progressive deprotonation reduces the repulsion of cationic species and enhances metal coordination on N and O donor reactive groups. It is noteworthy that for U(VI) and Cd(II) the pH-edges follow the same concave shape till pH_{eq} close to 4; the sorption capacities are close to 1.3 mmol U g^{-1} and 1.3 mmol Cd g^{-1}. Above pH 4, uranium sorption capacity tends to stabilize while for cadmium the sorption capacity sharply increases up to 1.9 mmol Cd g^{-1} at pH 4.5 and tends to stabilize at higher pH. The sorption capacity below pH 2.5 remains very low (lower than 0.3 mmol metal g^{-1}) because of the strong protonation of the sorbent. In the case of Hg(II) binding, the pH-edge is completely different in shape (convex form) with a significant and progressive increase of the sorption capacity up to pH 2.5; above this value the sorption capacity smoothly increases up to pH 4.5 before stabilizing (around 1.6–1.7 mmol Hg g^{-1}). Figure AM6 (see AMS) shows the pH variation during metal sorption. In most cases, the pH tends to slightly decrease (ΔpH below 0.9 unit). Figure AM7 (see AMS) plots the logarithm of the distribution coefficient, K_d (L g^{-1}) = q_{eq}/C_{eq}, defined as the ratio of sorption capacity to residual metal concentration ($K_d = q_{eq}/C_{eq}$) versus equilibrium pH. Regardless of the metal, two sections can be identified: (a) linear increase of the log K_d with the pH, followed by (b) a stabilization region. The correlations reported in Figure AM7 are limited to the linear sections; they show that the slope of the curves is systematically close to 0.5. In ion-exchange systems, this is frequently associated to the stoichiometry of ion-exchange of 2 protons per metal ion. The pH-edges are shifted toward higher pH values according the series: Hg(II) ≪ U(VI) < Cd(II). Comparing the ionic properties of these metal ions (Table AM10, see AMS), it was not possible establishing a clear correlation between pH-edge shifts and solubility, radius of hydrated species or softness. The speciation of metal ions may affect the binding of metal in relation with deprotonation and protonation of reactive groups. It is noteworthy that Hg(II) forms stable complexes with chloride ions (including $HgCl_2$, $HgCl_3^-$ and $HgCl_4^{2-}$, depending on pH and concentrations of Hg(II) and Cl^-) contrary to Cd(II) (which remains free). Figure AM8 (see AMS) shows the speciation of the three metal ions under the experimental conditions selected for the pH study. While U(VI) and Cd(II) are present in acidic solutions as neutral or cationic species (with electrostatic repulsion on protonated amine groups), mercury forms anionic species (below pH 2.5) that can bind to protonated amine groups. This explains the relatively more efficient binding of Hg(II) in acidic solutions compared with U(VI) and Cd(II).

The superimposition of the curves for duplicated experiments shows the good reproducibility of sorption properties and material synthesis (Fig. 1).

Sorption mechanisms

From FTIR and XPS analyses, combined with the interpretation of pH effect it is possible suggesting that the sorption of metal ions proceeds through

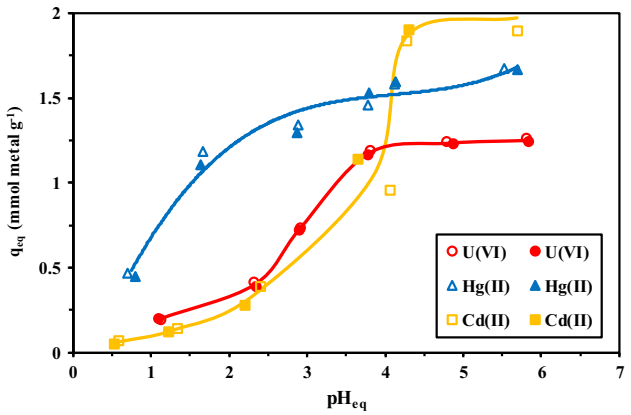

Figure 1 Effect of pH on U(VI), Hg(II) and Cd(II) sorption capacities using HAHZ-MG-CH sorbent (C_0: 70 mg metal L^{-1}, i.e., 0.294 mmol U L^{-1}, 0.349 mmol Hg L^{-1} and 0.623 mmol Cd L^{-1}; sorbent dosage, SD: 200 mg L^{-1}; contact time: 48 h; duplicated series: filled and opened symbols).

different mechanisms depending on the pH and the reactive groups effectively involved in metal binding.

At low pH (most acidic solutions, below pH 2), the sorbent is completely protonated. Metal binding may only occurs through ion-exchange mechanism. However, the repulsion effect (positively charged surface) limits the sorption of metal cations; the sorption remains very low.

With the increase of the pH, functional groups progressively deprotonate and electron pairs on chelating groups (bearing N and O donor groups) become available on the sorbent [63, 64]. It is noteworthy that the tautomerization effect on amide and imine groups (see Section IV, AMS) makes possible the formation of two types of complexes (monodentate and bidentate) with positively charged species.

When the pH increases above pH_{PZC}, the sorbent becomes deprotonated, metal species can be bound through chelation mechanisms but also through electrostatic attraction of metal cations with negatively charged functional groups [25].

These conclusions are supported by FTIR analysis (with the shifts of NH, NH_2, and OH peaks and their decreasing intensity after metal sorption). These mechanisms are also confirmed by XPS analysis trough:

(a) the disappearance of carbonyl functions (due to tautomerization with the amine moiety, and to the interaction with metal ions),

(b) the sharing of electrons on amine moieties during metal sorption (peak at 404.74 eV and 400.36 eV), and

(c) the appearance of a new peak of O 1s (which emphasizes the sharing of electrons from OH, O– during metal binding). Scheme 2 summarizes the different modes of interactions between the sorbent and metal species.

Uptake kinetics

The uptake kinetics for the three metals show that sorption is fast under selected experimental conditions (C_0: 100 mg L^{-1}; SD: 200 mg L^{-1}, pH_0: 5) (Fig. 2). A contact time of 30 min is sufficient for achieving the equilibrium for Hg(II) while for U(VI) and Cd(II), the equilibrium is reached within 1 h of contact. This is consistent with the higher self-diffusivity of mercury ions in water compared to other metal ions (Table AM10, see AMS). The micron-size of sorbent particles may explain the favorable mass transfer properties. Depositing a thin layer of polymer at the surface of magnetite particles (during the co-precipitation step of the support) reduces the intraparticle diffusion length. The uptake kinetics may generally be controlled by different resistances to diffusion (bulk, film and intraparticle) and by the proper reaction rate [15]. Here, the fast kinetics allows neglecting the contribution of resistance to diffusion and the kinetics profiles have been modeled by the PFORE and PSORE models (Table AM1, see AMS). Figure 2 compares the modeling of kinetic profiles with the two models: the pseudo-first order rate equation fits better experimental data than the pseudo-second order rate equation (especially in the zone of highest curvature). Table 1 confirms this conclusion; in most cases, the correlation coefficients are higher for PFORE than for PSORE and the calculated values of equilibrium sorption capacities are closer than experimental values. In the case of Hg(II) sorption on activated carbon issued from pistachio wastes, Sajjadi et al. [15] obtained a better modeling of kinetic profiles with the PFORE. The fit of kinetics by PFORE or PSORE is frequently correlated to the predominance of physical or chemical interactions. In this study, the two models give very close fits and it is not possible accurately distinguishing between the two modes of interaction. This can be explained by the simultaneous contribution of different

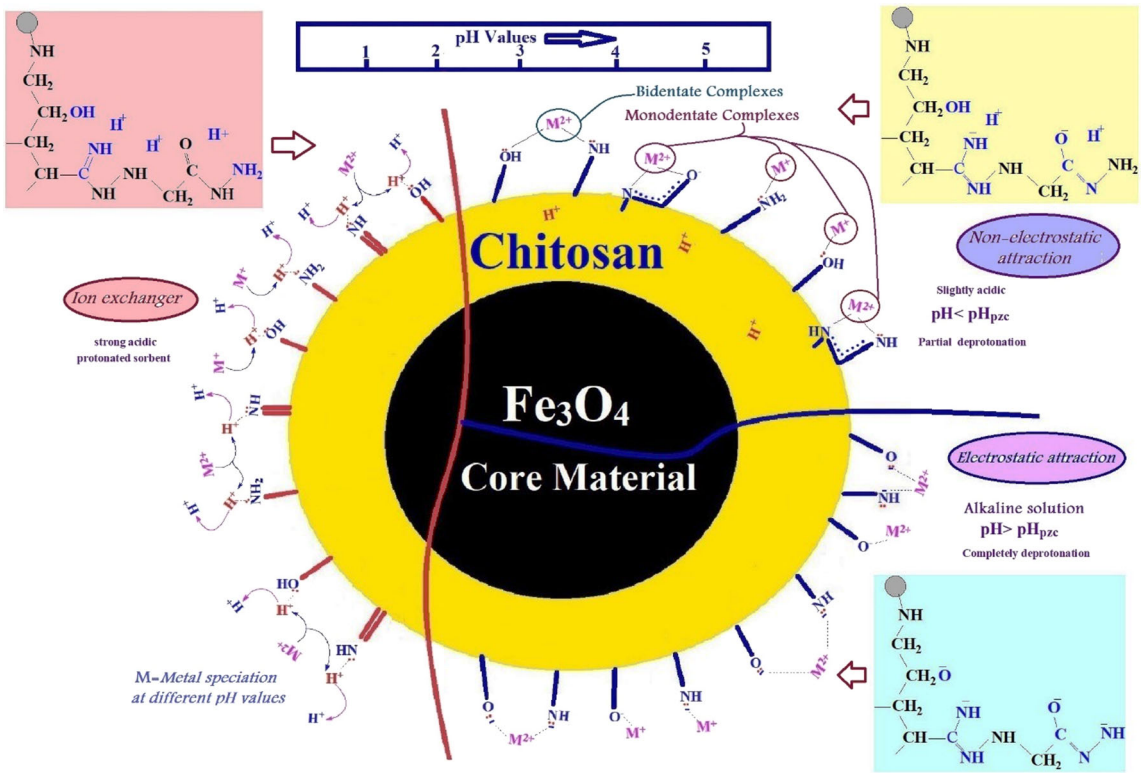

Scheme 2 Different modes of interaction between metal ions and the different reactive groups hold on HAHZ-MG-CH.

mechanisms associated to different reactive groups on the sorbent and to the effect of metal speciation that may involve different modes of interaction.

Figure AM9 (see AMS) shows another set of Hg(II) and Cd(II) uptake kinetics and Table AM11 (see AMS) reports the model parameters; in this case, the two models give very close fits.

Sorption isotherms

Figure 3 reports sorption isotherms at room temperature. The duplication of the isotherms confirms the reproducibility of sorption performance. The shape of sorption curves for both U(VI) and Hg(II) is characterized by a very favorable profile; the sorption of U(VI) and Hg(II) is almost irreversible (rectangular) with a steep initial slope followed by a saturation plateau. The plateau is reached for low residual concentrations, around 0.1–0.2 mmol L^{-1}. Similar favorable profiles were observed on activated carbons produced from different resources for heavy metal removal [15, 25], or with functionalized polymer brushes for uranium binding [11]. The sorption isotherm for Cd(II) is relatively different: the initial slope of the curve is less steep and a first pseudo-plateau of saturation is observed close to 2 mmol Cd g^{-1} before sorption capacity increases again for $C_{eq} > 1$ mmol Cd L^{-1}. Similar weaker affinity (marked by the initial slope of the curves), were observed in the case of Cd(II) uptake using some specific lignocellulosic biosorbents [25].

In Fig. 3, the solid line represents the fit of experimental data using the Langmuir equation (with the parameters summarized in Table 2). The determination coefficients (R^2) are close to 1 for U(VI) and Hg(II), while for Cd(II) the fit is less accurate (due to the 2 saturation plateaus reported above). The two-plateaus shape may correspond to the coexistence of two different sites with different affinity for target metal (or different binding mechanisms). An alternative modeling may consist of using a Langmuir two-site model [65]. Figure AM10 (see AMS) shows the comparison of the fits for linear and nonlinear regression determination of Langmuir parameters and the modeling of the isotherm for Cd(II) with the Langmuir bi-site equation. The nonlinear regression determination of Langmuir coefficients allows improving the fit of initial section of the isotherms in the case of highly favorable isotherms (vertical slope); in the case of Cd(II), the Langmuir bi-site equation

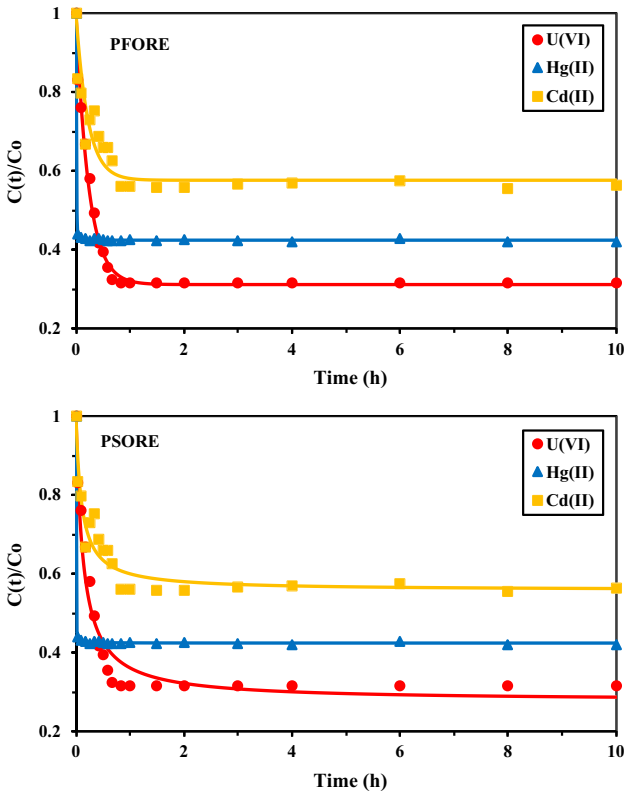

Figure 2 Uptake kinetics for U(VI), Hg(II) and Cd(II) recovery using HAHZ-MG-CH sorbent at pH 5—modeling with the PFORE and PSORE equations (pH_0: 5; C_0: 98.6 mg U L^{-1} or 109.5 mg Hg L^{-1} or 93.3 mg Cd L^{-1}; sorbent dosage, SD: 200 mg L^{-1}; T: 22 °C; solid lines represent the fitting of experimental profiles with relevant equations).

Table 1 Uptake kinetics for the recovery of U(VI), Hg(II) and Cd(II) using HAHZ-MG-CH sorbent at pH 5—modeling with the PFORE and PSORE equations

Model	Parameter	U(VI)	Hg(II)	Cd(II)
PFORE	$q_{eq,1}$ (mmol metal g^{-1})	1.427	1.571	1.761
	$k_1 \times 10^2$(min^{-1})	7.18	184.5	7.61
	R^2	0.963	1.0	0.910
PSORE	$q_{eq,1}$ (mmol metal g^{-1})	1.499	1.574	1.830
	$k_2 \times 10^2$ (L $mmol^{-1}$ min^{-1})	8.48	1033	8.65
	R^2	0.990	0.999	0.871
	$q_{eq,exp.}$ (mmol metal g^{-1})	1.420	1.582	1.803

also allows ameliorating the quality of the simulation at low residual concentration (Table AM12 and Figure AM10, see AMS).

The sorbent, at least at pH 5, shows preferences (maximum sorption capacity, mmol g^{-1}) according the series: Cd(II) (2.67) > Hg(II) (1.82) > U(VI) (1.55). The structure of the sorbent suggests some modes of

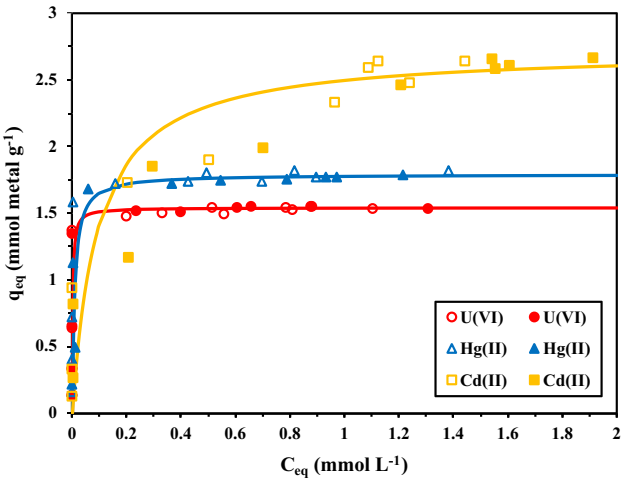

Figure 3 Sorption isotherms for U(VI), Hg(II) and Cd(II) recovery using HAHZ-MG-CH sorbent at pH 5 (T: 22 °C; SD: 300 mg L^{-1}; contact time: 48 h; duplicated series: filled and opened symbols; solid lines represent the fitting of experimental profiles with relevant equations).

Table 2 Sorption isotherms for the recovery of U(VI), Hg(II) and Cd(II) using HAHZ-MG-CH sorbent at pH 5—modeling with the Langmuir equation

Parameter	U(VI)	Hg(II)	Cd(II)
$q_{m,exp.}$ (mmol metal g^{-1})	1.55	1.82	2.67
$q_{m,calc.}$ (mmol metal g^{-1})	1.541	1.794	2.724
b (L $mmol^{-1}$)	502.5	118.4	10.93
R^{2a}	1.0	0.999	0.984

[a]R^2 determination coefficient calculated on linearized data (C_{eq}/q_{eq} = $f(C_{eq})$

interaction (chelation and ion-exchange) that may take place with metal ions based on:

(a) the arrangement of –NH and –OH functional groups (including tautomerization effect, see AMS),
(b) the protonation/deprotonation of reactive groups (especially NH_2 groups), and
(c) the speciation of metal ions (binding of mercury chloro-anionic species in acidic solutions; with a depleted effect at pH 5).

While U(VI) is considered a hard acid according Pearson's rules (HSAB) [66], Hg(II) and Cd(II) are classified as soft acids. The N-containing ligands (soft ligands) have a greater affinity for soft metals (such as Hg^{2+} or Cd^{2+}), while O-containing ligands prefer hard acids (such as UO_2^{2+}). This is hard to correlate with the current results. The sorbent bears both

N-based ligands and O-based ligands. Their structure being affected by protonation and tautomerization; this could explain the unexpected trend. This also means that the sorbent is more sensitive to other parameter or binding mechanisms. Table AM10 (see AMS) shows that the sorption capacities can be ranked according the reversal ranking of the radius (Å) of hydrated metal species: Cd(II) (0.95) < Hg(II) (1.01) < U(VI) (1.08). The next section addresses this selectivity issue through the study of metal binding from multi-metal solutions.

Table 3 reports some examples of sorption properties of alternative sorbents for U(VI), Hg(II) and Cd(II). The direct comparison of sorption capacities or kinetics (equilibrium time) is difficult because of different experimental conditions between the reported studies. However, this table gives an overview of the promising potential of HAHZ-MG-CH with reference to comparable sorbents. Though some sorbents have higher sorption capacities for individual selected metals, such as functionalized polymer brushes for U(VI) (up to 370 mg U g^{-1}) [11], HAHZ-MG-CH has remarkable sorption performances taking into account the sorption capacities for the three metals and the kinetic criterion (equilibrium time). This is a clear confirmation of the potential of this material for metal recovery: (a) relatively fast sorption, combined with (b) high sorption capacities. The selectivity and the capacity for recovering metal ions from complex solutions should be demonstrated, as well the possibility to desorb metal ions and recycle the sorbent.

Selectivity—sorption in multi-metal solutions

The sorption selectivity was investigated at different pH values with equimolar tri-metal solutions (0.6 mmol L^{-1}). The distribution coefficient ($K_{d,Me}$ = q_{eq}/C_{eq}, L g^{-1}) was determined for the different metal ions and the selectivity coefficient was determined by: SC(Me1/Me2) = $K_{d,Me1}/K_{d,Me2}$. Duplicated experiments are reported in Fig. 4 (plot of SC vs. pH for the different pairs of metals). Surprisingly, the sorbent had a marked preference for U(VI) and Hg(II) over Cd(II) in multi-metal solutions; this is contrary to the highest sorption capacities raised with Cd(II) in mono-metal solutions. The SC(U/Cd) and SC(Hg/Cd) reach a maximum at pH close to 3 with values ranging between 160 and 310. The sorbent can be efficiently used at pH 3 for separating Hg(II) and U(VI) from Cd(II).

The selectivity decreases at other pH values (below 2 and above 3.7) but the SC remains in the range 20–70 for U(VI) and Hg(II) against Cd(II). At pH 3, the predominant species are UO_2^{2+}, $HgCl_2$ and Cd^{2+}. At lower pH, cadmium predominates as $CdCl^+$ cationic species, which may compete with free uranyl species (Figure AM8, see AMS). For Hg(II), the formation of $HgCl_3^-$ offers the possibility of metal binding through electrostatic attraction on protonated amine groups: the SC(Hg/Cd) values remain at high levels (in the range 60–215) because of the limited competition of protonated $CdCl^+$ species with anionic chloro-complexes of Hg(II). At higher pH values (pH 4–4.5), the SC values decrease again due to the competition of Cd^{2+} species and neutral ($HgCl_2$) or cationic $HgCl(OH)^+$ species and to cationic mononuclear or polynuclear species of uranyl.

The presence of ligands (Cl^- and NO_3^-) may affect the availability of metal ions for binding on sorbent reactive groups [67]. For example for soft acids, the relative strength of Cl-ligands is comparable to the strength of N-based ligands and stronger than O-based ligands. Comparing the sorption of uranyl species on amine groups of the cell wall of *Rhizopus arrhizus* in the presence of different metal cations, Tobin et al. [68] reported that the inhibition effect increases with the ionic radius of the metal and its ionic charge.

The SC(U/Hg) increases with pH: HAHZ-MG-CH has a preference for Hg(II) in acidic solutions due to the formation of chloro-anionic species, which are adsorbed on protonated amine groups while repulsing cationic U(VI) species. With the increase of the pH, anionic mercury species progressively disappear and the reactive groups are deprotonated; this enhances the sorption of uranyl species, which are preferentially sorbed than mercury chloride species ($HgCl_2$). However, the SC(U/Hg) never exceeds 2 (under selected experimental conditions); this means that the effective separation of the two metal ions remains difficult.

The cumulative sorption capacity (not shown) follows an increasing linear trend versus pH: $q_{m,total}$ = 0.222 pH_{eq} +0.423 (R^2: 0.948). At pH 4–5, the cumulative residual metal concentration ($C_{eq,\ total}$) is close (in the range 0.6–0.68 mmol metal L^{-1}) for the two series and the corresponding cumulative

Table 3 Comparison of sorption properties (q_m, mmol g^{-1}) with alternative sorbents

Metal	Sorbent	pH	Equilibrium time (min)	q_m	References
U(VI)	Amidoxime-based sorbent	4	60	1.57	[36]
	Picolylamine resin	5.3	120	2.31	[74]
	Phosphoryl grafted silica	5	20	1.92	[75]
	Magnetic graphene oxide	6	40	2.63	[76]
	β-Cyclodextrin functionalized silica gel	4.5	60–90	0.07	[77]
	Modified PAN/MCM-41	5	60–240	1.49	[78]
	Amberlite IRA-402	3	90	0.90	[79]
	Chlamydomonas reinhardtii	4.5	30	1.45	[80]
	C-coated magnetic LDH	6	60–120	0.73	[81]
	TEPA magnetic chitosan composite	4	30	1.67	[82]
	Modified cactus fibers	5–6	120–240	0.45	[83]
	Alginate beads	3	60–90	0.13	[84]
	Chitosan tripolyphosphate beads	5	6000	1.0	[85]
	HAHZ-MG-CH	5	60	1.55	This work
Hg(II)	Hybrid organic/inorganic silica	6	240	1.03	[86]
	Aminophosphonic acid-functionalized PAN fiber	6	60	1.74	[87]
	DETA-grafted magnetic GMA resin	4	300	2.6	[88]
	Quaternary amide-sulfonamide resin	4	15	3.0	[89]
	Pistachio wood activated carbon	7	90	1.0	[15]
	Clay nanocomposites	7	60	0.42	[90]
	Ca-alginate beads	3.3	120	1.4	[91]
	Ca-pectinate beads	3.3	120	1.7	[91]
	Ca-polygalacturonate beads	3.3	120	1.5	[91]
	Rice husk	5.5	90	0.17	[92]
	HAHZ-MG-CH	5	60	1.82	This work
Cd(II)	Rice husk	6	90	0.13	[92]
	Carboxylated corn stalk	5.8	60	0.42	[58]
	EDTA-treated *Saccharomyces cerevisiae*	5	60	0.29	[19]
	Ca-alginate beads	6	480	0.28	[93]
	Ca-alginate beads/*Fucus vesiculosus*	6	480	0.58	[93]
	DETA-functionalized HEMA-PGMA resin	5	50	0.32	[94]
	Methylphosphonic acid-functionalized PS resin	5	180	0.34	[95]
	Amberlite IR-120	4–8	300	0.9	[96]
	Crosslinked polyaminophosphonate	4	240	0.48	[97]
	Duolite ES 467 resin	4.8	90	0.15	[98]
	001 × 7 strong cationic resin	4–5	120	3.16	[99]
	Porous anion exchanger aminated chelating fibers	3	60	1.12	[100]
	HAHZ-MG-CH	5	60	2.67	This work

sorption capacity is in the range 1.41–1.48 mmol metal g^{-1}. The sorption capacities obtained in single-metal solutions for the same range of residual metal concentrations can be calculated around 1.54 mmol U g^{-1}, 1.82 mmol Hg g^{-1} and 2.10 mmol Cd g^{-1}. These values are comparable to the sorption capacity of HAHZ-MG-CH for U(VI); this means that the metals compete for the same reactive groups and that the preference for U(VI) limits and controls the global sorption capacity of the sorbent.

Figure AM11 (see AMS) shows the molar fractions of the three metal ions on the sorbent at different equilibrium pH values. This confirms that: (a) at low pH (i.e., 1.1) Cd(II) is almost not sorbed, and (b) the sorbent preferentially accumulates Hg(II) (compared to U(VI)). On the other hand, at pH close to 4.3, U(VI)

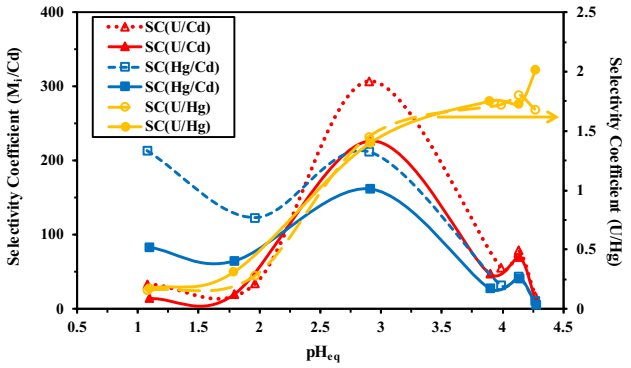

Figure 4 Sorption of U(VI), Hg(II) and Cd(II) on HAHZ-MG-CH sorbent from tri-component solutions—effect of equilibrium pH on selectivity coefficients (equimolar concentrations: C_0: 0.6 mmol of metal L^{-1}; SD: 360 mg L^{-1}; *T*: 22 °C; contact time: 48 h).

and Hg(II) are predominantly bound (44% and 41%, respectively) with Cd(II) representing about 15%.

Metal desorption and sorbent recycling

Metal desorption is an important criterion for evaluating the potential of a sorbent. Indeed, this controls the recovery and valorization of target metals but also the recycling of the sorbent, which controls the global competitiveness of the process. Metal desorption was operated using HCl solutions. In order to verify the stability of the sorbent, and more specifically the stability of magnetite core, the sorbent was mixed with HCl solutions of increasing concentrations. Figure AM12 (see AMS) shows the iron loss observed after 24 h of contact (under agitation). At 0.5 M HCl concentration, the loss of iron does not exceed 1.1%, and this concentration was used for further tests of metal desorption from loaded HAHZ-MG-CH material. Similar eluent was used for the desorption of metal ions from activated carbons [25]: acids are efficient eluents when metal ions are bound through either ion-exchange or chelation mechanisms. In the case of uranyl ions, HCl can be also used for recovering the metal from loaded sorbent [69–71]; however, sodium bicarbonate solutions have also been used for U(VI) desorption [72]. Figure AM13 (see AMS) compares the desorption kinetics for metal-loaded sorbent. The desorption of the three metal ions is achieved using 0.5 M HCl solutions, and the contact time for complete elution is systematically less than 1 h. Actually, a contact time of 20 min is sufficient for U(VI) and Cd(II) while 60 min are necessary for Hg(II). It is noteworthy that the ranking is reversed compared with sorption: faster Hg(II) sorption and slower Hg(II) desorption, compared with U(VI) and Cd(II): the ligand exchange is probably slower with Hg(II) that forms strong chloro-anionic complexes contrary to the other metals ions.

Table 4 compares the sorption and desorption efficiencies for U(VI), Hg(II) and Cd(II) for five successive cycles (average values and standard deviation). Regardless of the metal, the sorption and desorption efficiencies are decreasing with the number of cycles. However, even after 5 cycles, the loss in efficiency does not exceed 3.1%, 9.3% and 8.4% for the sorption of U(VI), Hg(II) and Cd(II), respectively. The loss in desorption efficiency is even lower after 5 cycles: less than 6.1%, 6.4%, and 4.8% for U(VI), Hg(II) and Cd(II), respectively (Figure AM14, see AMS). These results clearly demonstrate that the sorbent is stable. This is consistent with the FTIR characterization of the sorbent, which shows rather limited changes in the FTIR fingerprint of the sorbent after regeneration (Figure AM4, see AMS). The analysis of the eluates did not show significant amounts of iron (Figure AM12, see AMS) and the loss in efficiency remains limited along the five cycles. The sorbent can be re-used for a minimum of 5 cycles with high efficiency for the three metal ions.

In the case of heavy metal sorption and desorption on lignocellulosic-based biosorbents, Tran and Chao [25] observed a significantly lower decrease in performance between the first and the fifth cycle.

Treatment of real effluents

The sorbent was tested for the treatment of several groundwater samples. Table 5 reports the results obtained with the most contaminated sample. The sorption efficiency was determined for different pH values (acidified samples at pH 2 and 4, natural pH, i.e., 6.2, and at pH 7). As expected, the sorption efficiency increases with the pH. The sorbent reaches, under selected experimental conditions, sorption efficiencies higher than 95% for Cd(II), Pb(II) and Hg(II) at natural pH; the equilibrium pH value decreases to 5.88. However, for Zn(II), the efficiency does not exceed 65%. The sorption performance is even better at pH 4 (equilibrium pH decreased to 6): the sorption efficiency exceeds 99% for the three metals, while for Zn(II), the efficiency reaches 74%.

Table 4 Sorption and desorption cycles for U(VI), Hg(II) and Cd(II) using HAHZ-MG-CH—evolution of sorption and desorption efficiencies (average values and standard deviations)

Cycle	Sorption						Desorption					
	U(VI)		Hg(II)		Cd(II)		U(VI)		Hg(II)		Cd(II)	
	Av.	S.D.	Av.	S.D.	Av.	S.D.	Av.	S.D.	Av.	S.D.	Av.	S.D.
#1	99.26	0.03	92.05	0.82	98.78	0.05	99.40	0.26	97.16	0.26	99.11	1.09
#2	98.21	0.18	90.24	0.22	98.12	0.55	99.46	0.83	96.05	0.83	94.50	1.87
#3	97.85	0.08	89.09	0.75	96.04	0.30	98.68	0.21	96.10	0.21	93.81	5.33
#4	97.23	0.05	86.60	0.21	92.82	0.27	96.11	0.87	90.53	0.87	94.35	2.42
#5	96.19	0.32	83.54	1.01	90.46	1.52	93.42	0.75	90.93	0.75	94.34	3.68

Experimental conditions for sorption steps: C_0: 140 mg U or Hg L^{-1} or 80 mg Cd L^{-1}; SD: 410 mg L^{-1}; contact time: 24 h; pH_0: 5.0; T: 22 °C. Experimental conditions for desorption steps: 0.5 M HCl solutions; SD: 2000 mg L^{-1}; contact time: 2 h; T: 22 °C

Even at pH 7, the residual concentrations for Cd(II), Pb(II) and Hg(II) are higher that the allowed maximum levels (maximum level of concentration, MCL) for drinking water according the World Health Organization [1]. This means that the sorption process allowed a substantial abatement of metal pollution; however, this is insufficient for these metals for drinkable water regulations. The case of Zn(II) is little different since the MCL for this metal is relatively high (i.e., 5 mg L^{-1}) and higher than its initial concentration in the groundwater (i.e., 4.33 mg Zn L^{-1}).

The MCL for livestock feeds are: 0.05 mg Cd L^{-1}, 0.01 mg Hg L^{-1}, 24 mg Zn L^{-1} and 0.1 mg Pb L^{-1} [73]. This means that at "natural" pH and under selected experimental conditions, the treated water is proper for livestock feed. Mercury is not reported in the recommended levels for irrigation uses in the FAO list; for other target metals, the MCL are fixed to: 0.01 mg Cd L^{-1}, 2 mg Zn L^{-1} and 5 mg Pb L^{-1}. The recommended values are thus systematically respected regardless of the pH, under selected experimental conditions (SD: 5 g L^{-1}).

Conclusion

A new sorbent (HAHZ-MG-CH) has been reproducibly synthesized by grafting hydrazide groups onto composite magnetite-chitosan microparticles. The chemical analysis shows a high content of amine groups (close to 10.9 mmol N g^{-1}). The successive steps in the synthesis procedure have been confirmed using FTIR spectrometry and the morphological/structural properties have been characterized by SEM, TEM and BET analyses (specific surface area close to 12 m^2 g^{-1}). The magnetite core represents about 35–36% (measured by TGA analysis and degradation at 700 °C). The pH of zero charge (pH_{ZPC}) is close to 5.6, making the sorbent positively charged in acidic solutions. The sorption mechanism for U(VI), Hg(II) and Cd(II) is associated to the presence of –NH and –OH groups (confirmed by XPS analysis) and the sorption is controlled by the pH through multiple effects induced by protonation/deprotonation of reactive groups and specific ionic properties of target metals (including speciation effects). The sorption of mercury in HCl solutions is due to the formation of chloro-anionic species that can bind to protonated amine groups at low pH values, contrary to the other metals that are negligibly sorbed in acidic solutions. The sorption capacity increases with pH and the sorbent exhibits high sorption capacities for selected metals according the series: Cd(II) > Hg(II) > U(VI). However, the sorption from multi-metal (equimolar) solutions shows significantly different preferences. The sorbent is highly selective to Hg(II) and U(VI) versus Cd(II) (regardless of the pH, though the highest selectivity coefficients were obtained at pH 3). On the other side, the preference between Hg(II) and U(VI) is reversed by the pH: in acidic solutions (i.e., pH 2.5) HAHZ-MG-CH preferentially sorbs Hg(II). In less acidic solutions (i.e., pH 4), the sorbent has a higher affinity for U(VI). This modularity in preferences agrees with HSAB rules and the speciation of metal ions (in relation with protonation of amine functions).

The metals can be readily desorbed from the loaded sorbent using 0.5 M HCl solutions: the material is stable (less than 1.1% of iron is released from magnetite core). The sorption and desorption properties are maintained for at least five sorption/

Table 5 Application of the sorption process for the treatment of real effluents—pH effect on sorption performance using HAHZ-MG-CH sorbent (C_0: 2.08 mg Cd L^{-1}, 4.33 mg Zn L^{-1}, 1.01 mg Pb L^{-1}, 0.88 mg Hg L^{-1})

pH[a]	Metal	C_{eq} (mg L^{-1})	MCL[b] (mg L^{-1})	Removal efficiency (%)	C_0/MCL ratio	C_{eq}/MCL ratio
2 [2.33]	Cd(II)	1.85	0.003	11.0	693	617
	Zn(II)	3.22	5	25.8	0.87	0.64
	Pb(II)	0.52	0.01	48.3	101	52
	Hg(II)	0.76	0.002	13.2	440	382
4.0 [4.54]	Cd(II)	0.86	0.003	58.9	693	285
	Zn(II)	2.31	5	46.7	0.87	0.46
	Pb(II)	0.20	0.01	80.1	101	20
	Hg(II)	0.11	0.002	87.3	440	56
6.2 (natural value) [5.88]	Cd(II)	0.10	0.003	95.1	693	34
	Zn(II)	1.52	5	64.9	0.87	0.30
	Pb(II)	0.03	0.01	97.0	101	3
	Hg(II)	0.006	0.002	99.3	440	3
7.0 [6.0]	Cd(II)	0.006	0.003	99.7	693	2
	Zn(II)	1.12	5	74.1	0.87	0.22
	Pb(II)	0.01	0.01	99.0	101	1
	Hg(II)	0.005	0.002	99.4	440	2.5

Experimental conditions: SD: 5 g L^{-1}, contact time: 1 h; T: 22 °C

[a]pH: into bracket [equilibrium pH]

[b]MCL: maximum concentration level defined by WHO regulations

desorption cycles with a loss of efficiency generally lower than 8%.

The sorbent is successfully used for treating a metal-contaminated groundwater. High removal efficiencies (which are controlled by the pH) are observed for Hg(II), Cd(II), Pb(II) (and Zn(II) to a lesser extent). However, under selected experimental conditions, the treated water exceeds the maximum concentration levels (MCL) assigned for drinking water. The use of the sorbent at the natural pH allows decontaminating the groundwater at levels compatible with livestock drinking water and for irrigation purpose.

Acknowledgements

Yuezhou Wei and Xinpeng Wang thank the financial support of NSFC Projects (No.11675102, No.21866007). Eric Guibal and Mohammed Hamza acknowledge the Franco-Egyptian IMHOTEP program (Project MetalValor) (funded by French Government through Institut Français d'Egypte and Egyptian Government through Science and Technology Development fund from Egyptian Academy of Science and Technology). The authors are also grateful to the China Science and Technology Exchange Center (CSTEC) through Talented Young Scientists Program (TYSP) for the post-doc fellowship of Mohammed F. HAMZA (Teaching assistant position) at School of Resources, Environment and Materials—Guangxi University.

Electronic supplementary material: The online version of this article (https://doi.org/10.1007/s10853-019-04235-8) contains supplementary material, which is available to authorized users.

References

[1] WHO (2011) Guidelines for drinking-water quality. World Health Organization, Geneva

[2] Kavak D (2013) Removal of lead from aqueous solutions by precipitation: statistical analysis and modeling. Desalin Water Treat 51:1720–1726

[3] Wilson AM, Bailey PJ, Tasker PA, Turkington JR, Grant RA, Love JB (2014) Solvent extraction: the coordination chemistry behind extractive metallurgy. Chem Soc Rev 43:123–134

[4] Lai YC, Lee WJ, Huang KL, Wu CM (2008) Metal recovery from spent hydrodesulfurization catalysts using a combined acid-leaching and electrolysis process. J Hazard Mater 154:588–594

[5] Otrembska P, Gega J (2016) Separation of nickel(II) and cadmium(II) ions with ion-exchange and membrane processes. Sep Sci Technol 51:2675–2680

[6] Kabay N, Demircioglu M, Yayli S et al (1998) Recovery of uranium from phosphoric acid solutions using chelating ion-exchange resins. Ind Eng Chem Res 37:1983–1990

[7] Cao Q, Liu Y, Kong X, Zhou L, Guo H (2013) Synthesis of phosphorus-modified poly(styrene-co-divinylbenzene) chelating resin and its adsorption properties of uranium(VI). J Radioanal Nucl Chem 298:1137–1147

[8] Li C, Duan HD, Wang XJ, Meng X, Qin DW (2015) Fabrication of porous resins via solubility differences for adsorption of cadmium (II). Chem Eng J 262:250–259

[9] Shao GL, Xiao JF, Tian ZH, Huang JJ, Yuan SG (2018) Preparation and characterization of polyphenylene sulfide-based chelating resin-functionalized 2-amino-1,3,4-thiadiazole for selective removal Hg(II) from aqueous solutions. Polym Adv Technol 29:1030–1038

[10] Cai Z, Song X, Zhang Q, Liu Y (2017) Amidoxime surface modification of polyindole nanofiber membrane for effective removal of Cr(VI) from aqueous solution. J Mater Sci 52:5417–5434. https://doi.org/10.1007/s10853-017-0786-2

[11] Chi F, Zhang S, Wen J, Xiong J, Hu S (2019) Functional polymer brushes for highly efficient extraction of uranium from seawater. J Mater Sci 54:3572–3585. https://doi.org/10.1007/s10853-018-3040-7

[12] Yang Z, Chen G, Weng H, Shen W, Huang Z, Lin M (2018) Efficient and selective separation of U(VI) and Th(IV) from rare earths using functionalized hierarchically mesoporous silica. J Mater Sci 53:3398–3416. https://doi.org/10.1007/s10853-017-1808-9

[13] Liu DJ, Ding CC, Chi FT et al (2019) Polymer brushes on graphene oxide for efficient adsorption of heavy metal ions from water. J Appl Polym Sci 136:48156

[14] Wu HY, Chi FT, Zhang S, Wen J, Xiong J, Hu S (2019) Control of pore chemistry in metal-organic frameworks for selective uranium extraction from seawater. Microporous Mesoporous Mater 288:109567

[15] Sajjadi SA, Mohammadzadeh A, Tran HN et al (2018) Efficient mercury removal from wastewater by pistachio wood wastes-derived activated carbon prepared by chemical activation using a novel activating agent. J Environ Manag 223:1001–1009

[16] Khamirchi R, Hosseini-Bandegharaei A, Alahabadi A et al (2018) Adsorption property of Br-PADAP-impregnated multiwall carbon nanotubes towards uranium and its performance in the selective separation and determination of uranium in different environmental samples. Ecotoxicol Environ Saf 150:136–143

[17] Carro L, Barriada JL, Herrero R, de Vicente MES (2011) Adsorptive behaviour of mercury on algal biomass: competition with divalent cations and organic compounds. J Hazard Mater 192:284–291

[18] Sinha A, Pant KK, Khare SK (2012) Studies on mercury bioremediation by alginate immobilized mercury tolerant *Bacillus cereus* cells. Int Biodeterior Biodegrad 71:1–8

[19] Dutta A, Zhou LP, Castillo-Araiza CO, De Herdt E (2016) Cadmium(II), lead(II), and copper(II) biosorption on Baker's yeast (*Saccharomyces cerevesiae*). J Environ Eng 142:C6015002

[20] Safonov A, Tregubova V, Ilin V et al (2018) Comparative study of lanthanum, vanadium, and uranium bioremoval using different types of microorganisms. Water Air Soil Pollut 229:82

[21] Hu L-Q, Dai L, Liu R, Si C-L (2017) Lignin-graft-poly(-acrylic acid) for enhancement of heavy metal ion biosorption. J Mater Sci 52:13689–13699. https://doi.org/10.1007/s10853-017-1463-1

[22] Zhang D, Xiao J, Guo Q, Yang J (2019) 3D-printed highly porous and reusable chitosan monoliths for Cu(II) removal. J Mater Sci 54:6728–6741. https://doi.org/10.1007/s10853-019-03332-y

[23] Wei J, Yang Z, Sun Y et al (2019) Nanocellulose-based magnetic hybrid aerogel for adsorption of heavy metal ions from water. J Mater Sci 54:6709–6718. https://doi.org/10.1007/s10853-019-03322-0

[24] Vijayaraghavan K, Rangabhashiyam S, Ashokkumar T, Arockiaraj J (2016) Mono- and multi-component biosorption of lead(II), cadmium(II), copper(II) and nickel(II) ions onto coco-peat biomass. Sep Sci Technol 51:2725–2733

[25] Tran HN, Chao HP (2018) Adsorption and desorption of potentially toxic metals on modified biosorbents through new green grafting process. Environ Sci Pollut Res 25:12808–12820

[26] Vold IMN, Varum KM, Guibal E, Smidsrod O (2003) Binding of ions to chitosan—selectivity studies. Carbohydr Polym 54:471–477

[27] Roberts GAF (1992) Chitin chemistry. The Macmillan Press Limited, London

[28] Guibal E (2004) Interactions of metal ions with chitosan-based sorbents: a review. Sep Purif Technol 38:43–74

[29] Giraldo JD, Rivas BL, Elgueta E, Mancisidor A (2017) Metal ion sorption by chitosan-tripolyphosphate beads. J Appl Polym Sci 134, 45511

[30] Ruiz MA, Sastre AM, Guibal E (2002) Pd and Pt recovery using chitosan gel beads: I. Influence of drying process on diffusion properties. Sep Sci Technol 37:2143–2166

[31] Djelad A, Morsli A, Robitzer M, Bengueddach A, di Renzo F, Quignard F (2016) Sorption of Cu(II) ions on chitosan-zeolite X composites: impact of gelling and drying conditions. Molecules 21:109

[32] Wan M-W, Kan C-C, Rogel BD, Dalida MLP (2010) Adsorption of copper (II) and lead (II) ions from aqueous solution on chitosan-coated sand. Carbohydr Polym 80:891–899

[33] Meng J, Cui J, Yu J et al (2018) Preparation of green chelating fibers and adsorption properties for Cd(II) in aqueous solution. J Mater Sci 53:2277–2289. https://doi.org/10.1007/s10853-017-1653-x

[34] Javadian H, Ghaemy M, Taghavi M (2014) Adsorption kinetics, isotherm, and thermodynamics of Hg^{2+} to polyaniline/hexagonal mesoporous silica nanocomposite in water/wastewater. J Mater Sci 49:232–242. https://doi.org/10.1007/s10853-013-7697-7

[35] Hamza MF, Wei Y, Mira HI, Abdel-Rahman AAH, Guibal E (2019) Synthesis and adsorption characteristics of grafted hydrazinyl amine magnetite-chitosan for Ni(II) and Pb(II) recovery. Chem Eng J 362:310–324

[36] Hamza MF, Roux J-C, Guibal E (2018) Uranium and europium sorption on amidoxime-functionalized magnetic chitosan micro-particles. Chem Eng J 344:124–137

[37] Hamza MF, Abdel-Rahman AAH (2015) Extraction studies of some hazardous metal ions using magnetic peptide resins. J Dispers Sci Technol 36:411–422

[38] Mahdavinia GR, Shokri E (2017) Synthesis and characterization of magnetic amidoximated chitosan-g poly (polyacrylonitrile)/laponite RD nanocomposites with enhanced adsorption capacity for Cu^{2+}. Turk J Chem 41:135–152

[39] Varma AJ, Deshpande SV, Kennedy JF (2004) Metal complexation by chitosan and its derivatives: a review. Carbohydr Polym 55:77–93

[40] Elwakeel KZ, Atia AA (2014) Uptake of U(VI) from aqueous media by magnetic Schiff's base chitosan composite. J Clean Prod 70:292–302

[41] Liang W, Li ML, Zhang ZQ et al (2018) Decontamination of Hg(II) from aqueous solution using polyamine-co-thiourea inarched chitosan gel derivatives. Int J Biol Macromol 113:106–115

[42] Merrifield JD, Davids WG, MacRae JD, Amirbahman A (2004) Uptake of mercury by thiol-grafted chitosan gel beads. Water Res 38:3132–3138

[43] Roosen J, Binnemans K (2014) Adsorption and chromatographic separation of rare earths with EDTA- and DTPA-functionalized chitosan biopolymers. J Mater Chem A 2:1530–1540

[44] Hamza MF, Aly MM, Abdel-Rahman AAH et al (2017) Functionalization of magnetic chitosan particles for the sorption of U(VI), Cu(II) and Zn(II)—hydrazide derivative of glycine-grafted chitosan. Materials 10:539–560

[45] Lopez-Ramon MV, Stoeckli F, Moreno-Castilla C, Carrasco-Marin F (2009) On the characterization of acidic and basic surface sites on carbons by various techniques. Carbon 37:1215–1221

[46] Ho YS, McKay G (1999) Pseudo-second order model for sorption processes. Process Biochem 34:451–465

[47] Crank J (1975) The mathematics of diffusion. Oxford University Press, Oxford

[48] Foo KY, Hameed BH (2010) Insights into the modeling of adsorption isotherm systems. Chem Eng J 156:2–10

[49] Freundlich HMF (1906) Uber die adsorption in lasungen. Z Phys Chem 57:385–470

[50] Lau KKS, Gleason KK (2006) Particle surface design using an all-dry encapsulation method. Adv Mater 18:1972–1977

[51] Teng C-C, Ma C-CM, Lu C-H et al (2011) Thermal conductivity and structure of non-covalent functionalized graphene/epoxy composites. Carbon 49:5107–5116

[52] Desimoni E, Brunetti B (2015) X-ray photoelectron spectroscopic characterization of chemically modified electrodes used as chemical sensors and biosensors: a review. Chemosensors 3:70–117

[53] Hernan L, Morales J, Santos J, Espinos JP, Gonzalez-Elipe AR (1998) Preparation and characterization of diamine intercalation compounds of misfit layer sulfides. J Mater Chem 8:2281–2286

[54] Liu CK, Bai RB, Ly QS (2008) Selective removal of copper and lead ions by diethylenetriamine-functionalized adsorbent: behaviors and mechanisms. Water Res 42:1511–1522

[55] Deng SB, Bai RB, Chen JP (2003) Aminated polyacrylonitrile fibers for lead and copper removal. Langmuir 19:5058–5064

[56] Dong T, Yang L, Pan F et al (2017) Effect of immobilized amine density on cadmium(II) adsorption capacities for ethanediamine-modified magnetic poly-(glycidyl methacrylate) microspheres. J Magn Magn Mater 427:289–295

[57] Lv L, Zhang J, Yuan S et al (2016) Enhanced adsorption of Cu(II) ions on chitosan microspheres functionalized with polyethylenimine-conjugated poly(glycidyl methacrylate) brushes. RSC Adv 6:78136–78150

[58] Zheng L, Peng D, Meng P (2018) Promotion effects of nitrogenous and oxygenic functional groups on cadmium (II) removal by carboxylated corn stalk. J Clean Prod 201:609–623

[59] Xu Y, Zeng XB, Luo GQ, Xu YQ, Li X, Yao H (2018) Study on the effects of carrier and modifier on mercury adsorption behavior over halides modified sorbents using temperature programmed desorption method. Fuel Process Technol 178:293–300

[60] Yamashita T, Hayes P (2008) Analysis of XPS spectra of Fe^{2+} and Fe^{3+} ions in oxide materials. Appl Surf Sci 254:2441–2449

[61] Kyzas GZ, Siafaka PI, Pavlidou EG, Chrissafis KJ, Bikiaris DN (2015) Synthesis and adsorption application of succinyl-grafted chitosan for the simultaneous removal of zinc and cationic dye from binary hazardous mixtures. Chem Eng J 259:438–448

[62] Madrid JF, Nuesca GM, Abad LV (2014) Amine functionalized radiation-induced grafted water hyacinth fibers for Pb^{2+}, Cu^{2+} and Cr^{3+} uptake. Radiat Phys Chem 97:246–252

[63] Atta AM, Abdel-Rahman AAH, Hamza MF, El Aassy IE, Ahmed FY (2012) Effect of crosslinker chemical structure and monomer compositions on adsorption of uranium (VI) ions based on reactive crosslinked acrylamidoxime acrylic acid resins. J Dispers Sci Technol 33:490–496

[64] Hamza MF, El Aassy IE (2014) Solid phase extraction of uranium removal from underground water, Wadi Naseib, Southwestern Sinai, Egypt. Desalin Water Treat 52:331–338

[65] Escudero RR, Robitzer M, Di Renzo F, Quignard F (2009) Alginate aerogels as adsorbents of polar molecules from liquid hydrocarbons: hexanol as probe molecule. Carbohydr Polym 75:52–57

[66] Pearson RG (1966) Acids and bases. Science (New York, NY) 151:172–177

[67] Avery SV, Tobin JM (1993) Mechanisms of adsorption of hard and soft metal-ions to *Sacharromyces cerevisiae* and influence of hard and soft anions. Appl Environ Microbiol 59:2851–2856

[68] Tobin JM, Cooper DG, Neufeld RJ (1984) Uptake of metal-ions by *Rhizopus arrizus* biomass. Appl Environ Microbiol 47:821–824

[69] Basarir SS, Bayramgil NP (2013) The uranium recovery from aqueous solutions using amidoxime modified cellulose derivatives. IV. Recovery of uranium by amidoximated hydroxypropyl methylcellulose. Cellulose 20:827–839

[70] Metilda P, Sanghamitra K, Gladis JM, Naidu GRK, Rao TP (2005) Amberlite XAD-4 functionalized with succinic acid for the solid phase extractive preconcentration and separation of uranium(VI). Talanta 65:192–200

[71] Yang JB, Volesky B (1999) Biosorption of uranium on Sargassum biomass. Water Res 33:3357–3363

[72] Imam EA, El-Tantawy El-Sayed I, Mahfouz MG et al (2018) Synthesis of α-aminophosphonate functionalized chitosan sorbents: effect of methyl vs phenyl group on uranium sorption. Chem Eng J 352:1022–1034

[73] Ayers RS, Westcot DW (1994). In: FAO (ed) Food and agriculture organization of United Nations, Roma (Italy). http://www.fao.org/docrep/003/T0234E/T0234E00.htm. Accessed 20 June 2017

[74] Liu S, Yang Y, Liu T, Wu W (2017) Recovery of uranium(VI) from aqueous solution by 2-picolylamine functionalized polystyrene-co-maleic anhydride) resin. J Colloid Interface Sci 497:385–392

[75] Guo X, Feng Y, Ma L et al (2017) Phosphoryl functionalized mesoporous silica for uranium adsorption. Appl Surf Sci 402:53–60

[76] El-Maghrabi HH, Abdelmaged SM, Nada AA et al (2017) Magnetic graphene based nanocomposite for uranium scavenging. J Hazard Mater 322:370–379

[77] Liu H-J, Jing P-F, Liu X-Y, Du K-J, Sun Y-K (2016) Synthesis of beta-cyclodextrin functionalized silica gel and its application for adsorption of uranium(VI). J Radioanal Nucl Chem 310:263–270

[78] Bayramoglu G, Arica MY (2016) MCM-41 silica particles grafted with polyacrylonitrile: modification into amidoxime and carboxyl groups for enhanced uranium removal from aqueous medium. Microporous Mesoporous Mater 226:117–124

[79] Solgy M, Taghizadeh M, Ghoddocynejad D (2015) Adsorption of uranium(VI) from sulphate solutions using Amberlite IRA-402 resin: equilibrium, kinetics and thermodynamics study. Ann Nucl Energy 75:132–138

[80] Erkaya IA, Arica MY, Akbulut A, Bayramoglu G (2014) Biosorption of uranium(VI) by free and entrapped *Chlamydomonas reinhardtii*: kinetic, equilibrium and thermodynamic studies. J Radioanal Nucl Chem 299:1993–2003

[81] Zhang X, Wang J, Li R et al (2013) Preparation of Fe_3O_4@C@layered double hydroxide composite for magnetic separation of uranium. Ind Eng Chem Res 52:10152–10159

[82] Elwakeel KZ, Atia AA, Guibal E (2014) Fast removal of uranium from aqueous solutions using tetraethylenepentamine modified magnetic chitosan resin. Bioresour Technol 160:107–114

[83] Prodromou M, Pashalidis I (2013) Uranium adsorption by non-treated and chemically modified cactus fibres in aqueous solutions. J Radioanal Nucl Chem 298:1587–1595

[84] Bai J, Fan F, Wu X et al (2013) Equilibrium, kinetic and thermodynamic studies of uranium biosorption by calcium alginate beads. J Environ Radioact 126:226–231

[85] Sureshkumar MK, Das D, Mallia MB, Gupta PC (2010) Adsorption of uranium from aqueous solution using chitosan-tripolyphosphate (CTPP) beads. J Hazard Mater 184:65–72

[86] Perez-Quintanilla D, Sanchez A, Sierra I (2016) Preparation of hybrid organic-inorganic mesoporous silicas applied to mercury removal from aqueous media: influence of the synthesis route on adsorption capacity and efficiency. J Colloid Interface Sci 472:126–134

[87] Xu G, Wang L, Xie YJ, Tao ML, Zhang WQ (2018) Highly selective and efficient adsorption of Hg^{2+} by a recyclable aminophosphonic acid functionalized polyacrylonitrile fiber. J Hazard Mater 344:679–688

[88] Elwakeel KZ, Guibal E (2015) Selective removal of Hg(II) from aqueous solution by functionalized magnetic-macromolecular hybrid material. Chem Eng J 281:345–359

[89] Yavuz E, Turan GT, Alkazan S, Senkal BF (2015) Preparation of crosslinked quaternary amide-sulfonamide resin for removal of mercury ions from aqueous solutions. Desalin Water Treat 56:2145–2153

[90] Das S, Samanta A, Gangopadhyay G, Jana S (2018) Clay-based nanocomposites as recyclable adsorbent toward Hg(II) capture: experimental and theoretical understanding. ACS Omega 3:6283–6292

[91] Cataldo S, Gianguzza A, Pettignano A, Villaescusa I (2013) Mercury(II) removal from aqueous solution by sorption onto alginate, pectate and polygalacturonate calcium gel beads. A kinetic and speciation based equilibrium study. React Funct Polym 73:207–217

[92] Krishnani KK, Meng XG, Christodoulatos C, Boddu VM (2008) Biosorption mechanism of nine different heavy metals onto biomatrix from rice husk. J Hazard Mater 153:1222–1234

[93] Mata YN, Blazquez ML, Ballester A, Gonzalez F, Munoz JA (2009) Biosorption of cadmium, lead and copper with calcium alginate xerogels and immobilized *Fucus vesiculosus*. J Hazard Mater 163:555–562

[94] Trakulsujaritchok T, Noiphom N, Tangtreamjitmun N, Saeeng R (2011) Adsorptive features of poly(glycidyl methacrylate-co-hydroxyethyl methacrylate): effect of porogen formulation on heavy metal ion adsorption. J Mater Sci 46:5350–5362. https://doi.org/10.1007/s10853-011-5473-0

[95] Ferrah N, Abderrahim O, Amine Didi M, Villemein D (2013) Sorption efficiency of a new sorbent towards cadmium(II): methylphosphonic acid grafted polystyrene resins. J Chem 2013, 980825

[96] Demirbas A, Pehlivan E, Gode F, Altun T, Arslan G (2005) Adsorption of Cu(II), Zn(II), Ni(II), Pb(II), and Cd(II) from aqueous solution on amberlite IR-120 synthetic resin. J Colloid Interface Sci 282:20–25

[97] Al Hamouz OCS, Ali SA (2013) Removal of zinc and cadmium ions using a cross-linked polyaminophosphonate. J Macromol Sci A 50:375–384

[98] Rao KS, Chaudhury GR, Mishra BK (2010) Kinetics and equilibrium studies for the removal of cadmium ions from aqueous solutions using Duolite ES 467 resin. Int J Miner Process 97:68–73

[99] Wang F, Wang LJ, Li JS, Sun XY, Han WQ (2009) Adsorption behavior and mechanism of cadmium on strong-acid cation exchange resin. Trans Nonferrous Met Soc China 19:740–744

[100] Liu MQ, Tao ZA, Wang HC, Zhao F, Sun Q (2016) Preparation and characterization of a series of porous anion-exchanger chelating fibers and their adsorption behavior with respect to removal of cadmium(II). RSC Adv 6:115222–115237